Biosensors and Bioelectronics 143 (2019) 111601

Contents lists available at ScienceDirect

Biosensors and Bioelectronics

journal homepage: www.elsevier.com/locate/bios

ATMP-induced three-dimensional conductive polymer hydrogel scaffold for a novel enhanced solid-state electrochemiluminescence biosensor

Lian-Hua Xu[a], Jun-ji Li[a,**], Hai-Bo Zeng[a], Xue-Ji Zhang[a], Serge Cosnier[b], Robert S. Marks[c], Dan Shan[a,*]

[a] MIIT Key Laboratory of Advanced Display Materials and Devices, School of Environmental and Biological Engineering, Nanjing University of Science and Technology, Nanjing, 210094, China
[b] University of Grenoble Alpes-CNRS, DCM UMR 5250, F-38000, Grenoble, France
[c] Department of Biotechnology Engineering, Ben-Gurion University of the Negev, Beer-Sheva, Israel

ARTICLE INFO

Keywords:
Amino trimethylene phosphonic acid (ATMP)
Conductive hydrogel
Luminol derivative
Electrochemiluminescent (ECL)
Xanthine biosensor

ABSTRACT

Reliable and sensitive detection of xanthine has important medical and biological significance. In this work, a novel three-dimensional (3D) conductive polymer hydrogel of polyaniline (PAni) was feasibly prepared using aniline (Ani), amino trimethylene phosphonic acid (ATMP) and ammonium persulfate ($(NH_4)_2S_2O_8$) as monomer, gelatinizing agent and oxidizing agent, respectively. Protonation of aniline can be achieved by ATMP, inducing good conductivity of the obtained hydrogel. ATMP remained the chelating abilities in the conductive hydrogel, enabling further immobilization with silver nanoparticles (AgNPs) functionalized by a luminol derivative, N-(aminobutyl)-N-(ethylisoluminol) (ABEI). ABEI-Ag@PAni-ATMP exhibited an enhanced performance of solid-state electrochemiluminescence (ECL). Integrated with xanthine oxidase (XOD), the proposed biosensor can be applied in the detection of xanthine *via in-situ* generated hydrogen peroxide (H_2O_2), and present a low detection limit of 9.6 nM, a wide linear range (from 0.01 to 200 μM) and excellent stability.

1. Introduction

Xanthine is a product of purine degradation pathway and can be converted to uric acid under the catalysis of xanthine oxidase (XOD). Excessive accumulation of uric acid in the body will lead to gout. Therefore, the development of a simple, inexpensive, highly sensitive xanthine sensor has important medical and biological significance (Kalimuthu et al., 2012; Devi et al., 2012; Xue et al., 2019). Based on the formation of uric acid and hydrogen peroxide (H_2O_2) during the XOD-catalyzing reaction: Xanthine + $O_2 \xrightarrow{XOD}$ Uric acid + H_2O_2 (Wang et al., 2011), the detection of xanthine has been generally previously developed using electrochemical (EC) (Juskowiak, 2006), fluorescence (Flu) (Stulz et al., 2011) and surface-plasma resonance methods (Burge et al., 2006) As for the electrochemical detection of xanthine, the high overpotential for direct oxidation of H_2O_2 necessitated sensor operation at potential more than 0.3 V, and uric acid has a reducing property and is easily oxidized at a high potential (Shan et al., 2009a). Therefore, it is desirable to construct a xanthine biosensor which can effectively reduce/avoid the interference of uric acid. Exhibiting high sensitivity, wide dynamic response range, simplicity of operation, excellent controllability and low background noise, the electrochemiluminescence (ECL) technique has been widely applied into cell analysis and clinical diagnostics (Wang et al., 2015; Cai et al., 2017). Luminol or its derivates in the H_2O_2 ECL system is a relatively mature system. However, in the aforementioned systems, luminol or its derivatives are commonly dispersed within the electrolyte which could cause a waste of the luminophore and the electrolyte is easy to be contaminated. Therefore, a solid-state ECL biosensor is proposed as a more desirable system to determine xanthine. N-(aminobutyl)-N-(ethylisoluminol) (ABEI), a special derivative of luminol, has attracted wide interest in multiple fields (Jiang et al., 2016). Due to a greater spatial distance between the amino terminal and the aromatic ring of ABEI compared with luminol, the conjugating attraction effect towards amino group becomes weaker, which is beneficial to its functionalization or immobilization, thereby greatly reducing the space length between the luminescent label and the electrode, thus offering improved ECL efficiency (Yang et al., 2017). In addition, Ag nanoparticles (Ag NPs) can catalyze the decomposition of H_2O_2 and the generation of hydroxyl radical (OH•), which further enhances the ECL intensity of ABEI (Jiang et al., 2016; Li et al., 2015). Thus, a solid-state ABEI-

* Corresponding author.
** Corresponding author.
E-mail addresses: junjili@njust.edu.cn (J.-j. Li), danshan@njust.edu.cn (D. Shan).

https://doi.org/10.1016/j.bios.2019.111601
Received 20 June 2019; Received in revised form 1 August 2019; Accepted 13 August 2019
Available online 16 August 2019
0956-5663/

functionalized Ag NPs (ABEI-Ag) ECL biosensor, exhibiting high sensitivity, reagent-saving property, and recyclability seems ideal to be developed for the determination of xanthine.

In order to optimize ECL detection, we realized the usefulness in constructing a proprietary solid-state luminescent material interface. Since conductive polymer hydrogels have similarities to native tissues, they can be used as an excellent matrix for enzyme adhesion in the fields of biosensing and drug/enzyme release (Abu-Rabeah et al., 2005; Jiang et al., 2018). Therefore, we designed a 3D conductive polymer hydrogel which is ideal for the immobilization of ABEI-Ag. Amino trimethylene phosphonic acid (ATMP), which possesses good chemical stability (melting point: 200 °C, boiling point: 746.2 °C), chelating ability and cost-efficiency, has successfully caught our consideration. Specifically, as a kind of acid, ATMP is a strong complexing agent for divalent cations with the morphology of a tripodal tetradentate formed by combining the central atom 'N' with three ligands 'metaphosphate group'. In the three phosphonic groups of ATMP, the phosphorus atom forms a σ bond with an oxygen atom in form of sp^3 orbital, a p-dπ bond, which is perpendicular to the P–O σ bond that is formed between $3d^0xz$ and 2pz as well as $3d^0xy$ and 2py (Hoffmann et al., 2012; Zhuang et al., 1985). Therefore, ATMP is more readily combined with a base to form a stable hydrogel precursor. Aniline (Ani) is easily protonated under acidic conditions to form a highly conductive polyaniline under the oxidation of a strong oxidizing agent. Using ATMP as a gelation agent and protonic acid dopant, Ani can be protonated, inducing good conductivity in the formed 3D conductive polymer hydrogel scaffold under the strong oxidation of $(NH_4)_2S_2O_8$ (PAni-ATMP). During the generating process of a 3D conductive polymer hydrogel, a maximum of three phosphoric acid groups of one ATMP molecule is able to interact with PAni though electrostatic interaction or an alternative N–H···O hydrogen bonding. Hence, it forms the basis of a xanthine biosensor using the said 3D conductive polymer hydrogel as matrix.

According to the above analysis, a novel solid-state ECL biosensor based on an ABEI-Ag decorated 3D PAni-ATMP conductive polymer hydrogel (ABEI-Ag@PAni-ATMP) was designed for the specific detection of xanthine using *in-situ* generated H_2O_2 as co-reactant under the catalysis of XOD (Scheme 1). XOD is a complex oxidoreductase enzyme with an active site composed of a molybdopterin unit and molybdenum (Mo) atom coordinated to terminal oxygen, sulfur atoms, and terminal hydroxide (Si et al., 2018). During the reaction of xanthine to uric acid, the oxygen on the molybdenum is firstly transferred to the xanthine molecule to form uric acid, and then the water molecule is added to the active intermediate to regenerate the active molybdenum center (S. Wang et al., 2019). The proposed 3D ABEI-Ag@PAni-ATMP conductive polymer hydrogel was explored for its performance potential in detecting trace xanthine from processed fresh fish tissue samples.

2. Experimental section

2.1. Chemicals and materials

N-(Aminobutyl)-N-(ethylisoluminol) (ABEI) was obtained from TCI Shanghai (China). Sodium chloride (NaCl), magnesium chloride ($MgCl_2$), Aniline (Ani) and amino trimethylene phosphonic acid (ATMP, 50 wt%) were bought from Shanghai Meryer Chemical Technology Co., Ltd (China). Ammonium persulfate ($(NH_4)_2S_2O_8$) was purchased from Shanghai Lingfeng Chemical Reagent Co., Ltd (China). Ethanol, hydrogen peroxide (H_2O_2) and sodium hydroxide (NaOH) were bought from Sinopharm Chemical Reagent Co., Ltd (China). Silver nitrate ($AgNO_3$), guanine (G), glutamic acid (Glu), uric acid (UA), and ascorbic acid (AA) were purchased from Sigma Aldrich (China). Xanthine was purchased from Shanghai Titan Scientific Co., Ltd (China). Xanthine oxidase (XOD) was bought from Shanghai Yuanye Biotechnology Co., Ltd. (China). All other chemicals were of analytical grade and used without further purification. Ultrapure water was used during the experiment. The phosphate buffer solution (PBS, 0.1 M, pH 8) was employed as a working buffer solution.

2.2. Apparatus

An UV–vis spectrophotometry (UV-3600, Shimadzu, Japan) was used for measuring the absorption spectra. A XL-30E scanning electron microscope (SEM) was served to investigate the detailed morphologies of the modified electrode. The MPI-EII multifunctional electrochemical and chemiluminescent analysis system (Xi'an Remex Analytical Instrument Co., Ltd., China) was used for ECL testing, and the photomultiplier tube were set at 1000 V, the magnification level was 2. The above research was carried out with the traditional three-electrode system. The Hg/Hg_2Cl_2 electrode, platinum wire electrode and glassy carbon electrodes (GCE) ($\Phi = 5$ mm) are the reference electrode, counter electrode, and working electrode respectively. ECL detection was studied at a scan rate of 50 mV s^{-1} within the scan range from 0 to 0.8 V. An Autolab PGSTAT30 (Eco Chemie) which was controlled by NOVA 1.10 software was applied for Electrochemical impedance spectroscopy (EIS) measurement. The Cell Disrupter (F6/10, Shanghai Jingxin Technology, China) was used to disperse and break fish cells. The Mix Smart (Mix-100, Hangzhou Allsheng Instruments Co.,Ltd, China) was served to homogenize the fish mixture solution.

2.3. Preparation of the PAni-ATMP conductive polymer hydrogel modified electrode

The ATMP-induced conductive polymer hydrogel was prepared as below: 0.46 mL 50 wt% ATMP aqueous solution (1.8×10^{-3} mol) and 0.115 mL Ani (1.3×10^{-3} mol) were initially dissolved into 1 mL of ultrapure water under sonication treatment until a transparent solution A was formed. Meanwhile, 0.0715 g of $(NH_4)_2S_2O_8$ (1.3×10^{-3} mol) was added into ultrapure water (0.5 mL) under sonication treatment until a transparent solution B was formed. Both solution A and B were stored at 4 °C. Then, solution B was added into solution A and allowed to mix well and react on a cleaned GCE for 30 min at 4 °C, the PAni-ATMP conducting hydrogels modified GCE was then obtained. Then, in order to remove oligomers, the obtained PAni-ATMP modified GCE was immersed in ultrapure water for about 30 min. Subsequently, the obtained PAni-ATMP modified GCE was dried in a drying oven at 40 °C.

2.4. Preparation of an ABEI-Ag luminophor

The detailed preparation process of ABEI-Ag luminophore was according to the literature with a slight modification (Li et al., 2018). Firstly, The ABEI was dissolved in 0.1 mM NaOH aqueous solution at a concentration of 20 mM and stored at 4 °C in a refrigerator. 1 mL of 10 mM $AgNO_3$ was added into a mixing solution containing 5 mL of ethanol and 2 mL of ultrapure water. After stirring for about 30 min, 1 mL of 20 mM ABEI NaOH aqueous solution was immediately added into the above solution, and then stirring for 12 h in darkness at ambient temperature. Finally, the ABEI-Ag luminophore was centrifuged and washed three times with ethanol and ultrapure water and dried in the vacuum freeze-dryer for further use.

2.5. Preparation of the ABEI-Ag@PAni-ATMP conducting hydrogel modified electrode

10 μL ABEI-Ag solution was taken out and dripped it on the PAni-ATMP modified GCE. After reacting for 12 h, the ABEI-Ag@PAni-ATMP conducting polymer hydrogel modified electrode was washed with ultrapure water and dried in a drying oven at 40 °C.

2.6. Construction of a xanthine electrochemiluminescence biosensor

10 μL of the XOD (2 mg/mL) was spread onto the surface of the ABEI-Ag@PAni-ATMP conductive polymer hydrogel modified electrode

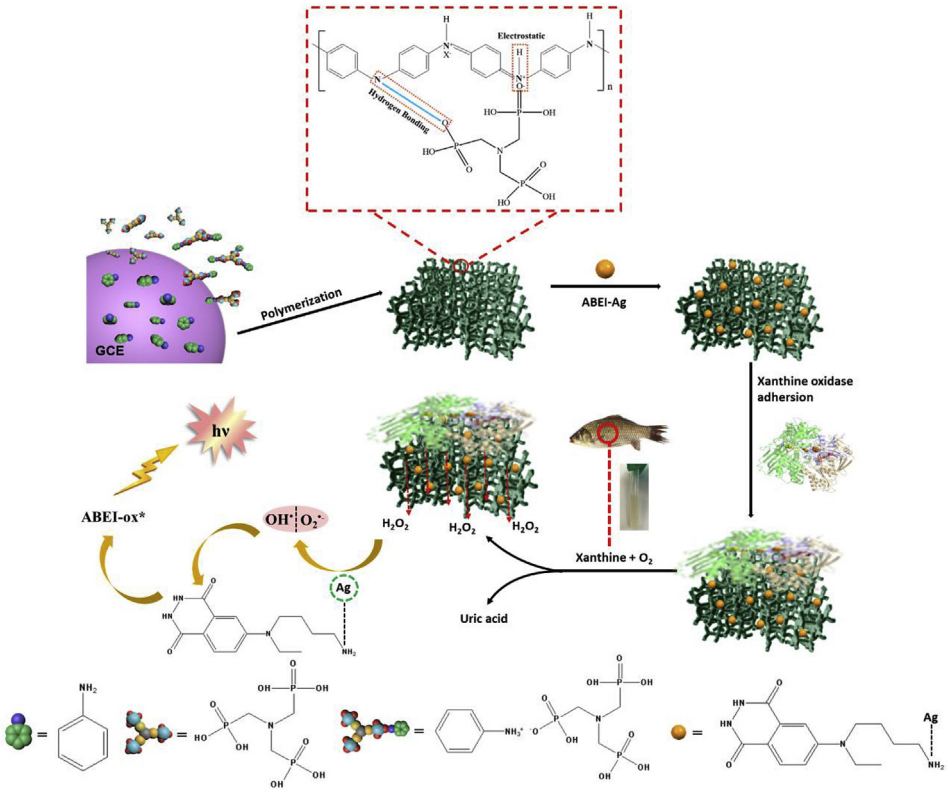

Scheme 1. Schematic illustration of the fabrication process of the ABEI-Ag@PAni-ATMP ECL biosensor for xanthine.

and dried at room temperature. Different concentrations of xanthine were added into 4 mL of PBS working buffer. In order to confirm the practical capability of our sensor, we used fish as a model sample to detect xanthine.

2.7. Preparation of the fish target sample

The fish meat was homogenized with a Cell Disrupter in 1:5 ratios (g/ml). The highly dispersed solution was then shaken for 10 min by Mix Smart and centrifuged to obtain a supernatant. 10 μL supernatant was added to 4 mL of PBS working buffer for detection.

3. Results and discussion

3.1. Characterization of PAni-ATMP and ABEI-Ag@PAni-ATMP

The stepwise materials were analyzed by UV–vis spectrophotometry during the formation of ATMP-induced conductive polymer hydrogel. As depicted in Fig. 1A, ATMP (curve a) and $(NH_4)_2S_2O_8$ (curve b) exhibited no significant peaks, while the Ani (curve c) showed two absorption peaks. The greater absorption peak was observed at about 230 nm, which stood for the E absorption band of benzene ring (Naqash and Majid, 2017). A moderate absorption peak appeared at about 285 nm, corresponding to the B absorption band of the benzene ring. When ATMP was added (curve d), the acid-base neutralization reaction between ATMP and oily basic Ani occurred. The solution became transparent and homogeneous (as shown in the insert Fig. 1A–a), reflecting the acid-base neutralization dominated by ATMP. Meanwhile, the p-π bonds formed by amino and benzene rings was destroyed, resulting in the decrease of the absorption peak at 285 nm and 230 nm. With the addition of $(NH_4)_2S_2O_8$, the PAni-ATMP gel was gradually formed (curve e). The mixture became olive green after about 15 min, (Fig. 1A–b). Meanwhile, the UV–vis absorption peaks of PAni-ATMP gel appeared at 446 and 720 nm, corresponding to the polaron-to-π* and π-to-polaron transitions, respectively, demonstrating the formation of PAni (Huang et al., 2015; Niu, 2006; Choi et al., 2018).

ATMP also played a key role in the construction of solid-state luminescent material interfaces. The remaining chelating abilities of ATMP in the conductive polymer hydrogel, was favorable for the further immobilization of ABEI-Ag. As can be shown in Fig. 1B, two characteristic bands of ABEI (curve a) appeared at 290 nm and 320 nm. The peak at 290 nm was caused by the conjugated K-band absorption peak of the carbonyl group and the benzene ring. In addition, the strong B-band at 320 nm was due to the π-π* transition and the overlap of the benzene rings (Jiang et al., 2016; Li et al., 2018). Interestingly enough, a new absorption band centered at 400–600 nm was observed in the absorption spectra of ABEI-Ag (curve b) compared with the absorption spectra of ABEI, indicating the successful synthesis of Ag NPs (Liu et al., 2018). There were five peaks on the UV–vis spectra of the proposed ABEI-Ag@PAni-ATMP (curve c). It was observed that the peak located at 400–600 nm corresponds to Ag NPs. Due to the interaction with the hydrogel network, a certain blue shift occurred in the absorption peaks at 290 nm. A peak at 320 nm corresponds to ABEI. Meanwhile, the characteristic peaks of PAni-ATMP was also maintained. Therefore, the ABEI-Ag was demonstrated to be successfully functionalized with the PAni-ATMP conductive polymer hydrogel.

The synthesized PAni-ATMP and ABEI-Ag@PAni-ATMP conductive polymer hydrogels were characterized by scanning electron microscopy (SEM) and transmission electron microscope (TEM). As can be seen in Fig. 1C and E, the surface of the PAni-ATMP gel showed a 3D porous and hierarchical network structure with pore size ranging from 0.02 to 1 μm. When ABEI-Ag was loaded, as shown in Fig. 1D and F, the 3D porous morphology was maintained and large numbers of ABEI-Ag nanoparticles with a diameter ranging from 10 to 20 nm were dispersed homogeneously within the 3D porous PAni-ATMP conductive polymer hydrogel.

XPS was performed to investigate the bonding configuration and chemical state in the proposed catalysts. The full XPS survey spectra of

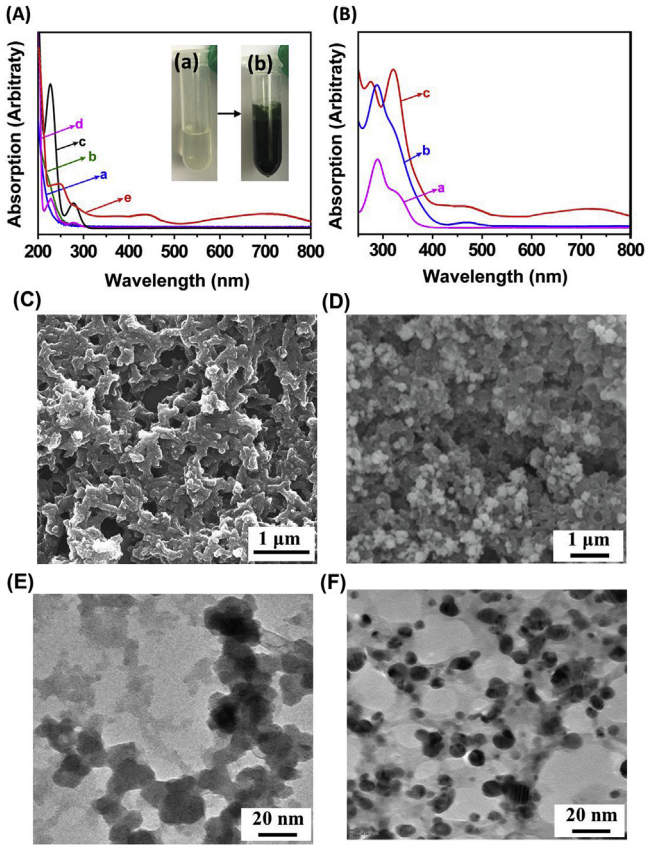

Fig. 1. (A) UV–vis absorption spectra of (a) ATMP, (b) $(NH_4)_2S_2O_8$, (c) Ani, (d) Ani-ATMP and (e) PAni-ATMP. Inset: the picture of (a) Ani-ATMP and (b) PAni-ATMP solutions. **(B)** UV–vis absorption spectra of (a) ABEI, (b) ABEI-Ag and (c) ABEI-Ag@PAni-ATMP. SEM images of **(C)** PAni-ATMP and **(D)** ABEI-Ag@PAni-ATMP. TEM images of **(E)** PAni-ATMP and **(F)** ABEI-Ag@PAni-ATMP.

PAni-ATMP and ABEI-Ag@PAni-ATMP (Fig. 2A) both show five main peaks of Ag 3d, N 1s, C 1s, and O 1s at 368.45 eV, 398.25 eV, 284.60 eV and 397.30 eV, respectively. For Ag 3d fine spectrum (Fig. 2B), the deconvoluted two sub-peaks located at 366.16 and 372.11 eV are the characteristic Ag^+ $3d_{5/2}$ and Ag^+ $3d_{3/2}$. In addition, two peaks at 366.80 and 372.71 eV corresponding to Ag $3d_{5/2}$ and Ag $3d_{3/2}$. This result is consistent with previous literature reports (Jiang et al., 2004). The N 1s XPS spectra of ABEI-Ag@PAni-ATMP was decomposed into three dominant peaks (Fig. 2C), which correspond to imine-like (=N-) structure (399.53 eV), amine-like nitrogen atoms (–NH–) (400.44 eV) and positively charged nitrogen (401.41 eV), respectively (Wu et al., 2006). The high-resolution XPS spectra of C 1s present four types of C species: C–C (284.64 eV), C=N (285.39 eV) and C–O (284.30 eV) and C=O (285.71 eV). The maximal peak centered at 284.64 was attributed to the C–C bond in ABEI. The component at 285.39 eV was associated with the C=N bond. The component at 284.30 eV was due to the exist of C–O bond. The characteristic peak of the C=O bond was attributed to the carbon atom in the carboxylic group (-COO-) of the ABEI oxidation product (He et al., 2011; Wu et al., 2006). The results supported that ABEI and its oxidation product coexisted on the surface of the ABEI-Ag@PAni-ATMP.

3.2. Electrochemical and ECL behavior of ABEI-Ag@PAni-ATMP for H_2O_2

Figure S2 shows the comparative CV curves of ABEI-Ag@PAni-ATMP conducting hydrogels modified electrodes in 0.1 M PBS solution in the (a) absence and (b) presence of 20 μM H_2O_2. No obvious peak can be observed in the absence of H_2O_2. In the presence of 20 μM H_2O_2, an oxidization peak at about 0.52 V correspond to the oxidation of Ag NPs which can be ascribed to the reduction of H_2O_2 (Z. Wang et al., 2019). Meanwhile, H_2O_2 decompose and generate hydroxyl radical ($OH^{\bullet}$) and then react with ABEI to promote the formation of excited-state oxidation products ABEI-ox* to emit the stronger ECL signal.

EIS was applied for characterizing the conductivities of materials and electrode surface modification. The Nyquist plot of the Ani-ATMP and the PAni-ATMP conductive polymer hydrogels modified GCE were displayed in Fig. 3A. Compared with the semicircular diameter obtained from Ani-ATMP (curve a), the semicircular diameter of PAni-ATMP modified GCE is significantly reduced (curve b), indicating that the copolymerized materials owned excellent conductivity, meanwhile reflecting the formation of conductive polyaniline network. The Nyquist plot of the ABEI-Ag@PAni-ATMP and the XOD modified ABEI-Ag@PAni-ATMP were displayed in Fig. S2. Compared with the semicircular diameter obtained from ABEI-Ag@PAni-ATMP (curve a), the semicircular diameter of XOD modified ABEI-Ag@PAni-ATMP is significantly increased (curve b), indicating the successful immobilization of XOD onto ABEI-Ag@PAni-ATMP conductive polymer hydrogel.

The ECL behaviors of ABEI-Ag@PAni-ATMP conductive hydrogel were investigated in 0.1 M PBS solution. In the absence of H_2O_2, no significant ECL signal was observed (Fig. 3B, curve a). In the presence of 20 μM H_2O_2, the light intensity of the cathode ECL signal reached approximately 6000 a.u., while the ECL peak was located at approximately 0.7 V (Fig. 2B, curve b). Inset of Fig. 2B displays the ECL-potential curves of (a) bare GCE, (b) PAni-ATMP, (c) ABEI-Ag and (d) ABEI-Ag@PAni-ATMP in PBS containing 20 μM H_2O_2. It was clear that the ECL intensity of ABEI-Ag@PAni-ATMP was comparatively stronger than that of ABEI-Ag in a homogeneous phase.

3.3. Analytical performance of the ABEI-Ag@PAni-ATMP conducting hydrogel-modified electrode for H_2O_2

H_2O_2 has great influence on the luminescence efficiency as the co-reaction reagent of the ABEI in ECL systems (Jiang et al., 2018). To investigate the sensitivity of the ABEI-Ag@PAni-ATMP conductive polymer hydrogel modified electrode toward H_2O_2, the ECL responses of the ABEI-Ag@PAni-ATMP for different concentrations of H_2O_2 ranging from 0.01 to 60 μM were recorded. As shown in Fig. S1A, with the addition of H_2O_2, the ECL signal consecutively increased. Moreover, two good linear segments were observed. The linear regression equation for the lower concentration (0.01 μM–1 μM) was I (a.u.) = 2204c − 164.9 (R = 0.996). Another linear regression equation for the higher concentration (1 μM–60 μM) was I (a.u.) = 183.4c + 2013.3 (R = 0.988). The detection limit is calculated to be 6.8 nM (ratio of signal to noise, S/N = 3). Comparisons of the linear range and the detection limit with other reported H_2O_2 sensors were summarized in Table S1. Obviously, the ABEI-Ag@PAni-ATMP conductive polymer hydrogel sensor showed a relatively low detection limit. Besides, as shown in Fig. S1B, the ABEI-Ag@PAni-ATMP conductive polymer hydrogel modified electrode showed constant and stable signals toward 20 μM H_2O_2 with a relative standard deviation (RSD) of 0.988%.

3.4. Analytical performance of the XOD modified ABEI-Ag@PAni-ATMP conducting hydrogel electrode for xanthine

Meanwhile, a sensitive detection of xanthine was also achieved. 10 μL of the XOD solution was spread onto the surface of the ABEI-Ag@PAni-ATMP conductive polymer hydrogel modified electrode to investigate the sensitivity toward xanthine, the ECL responses of the ABEI-Ag@PAni-ATMP for different concentration of xanthine ranging from 0.01 to 200 μM were recorded. As shown in Fig. 3C, a fine linear correlation was illustrated with the xanthine concentration increase. For the lower concentration (0.01–1 μM), the linear regression equation and squared correlation coefficient were I (a.u.) = 1928c − 96 and 0.999, respectively. For the higher concentration (1–200 μM), the linear

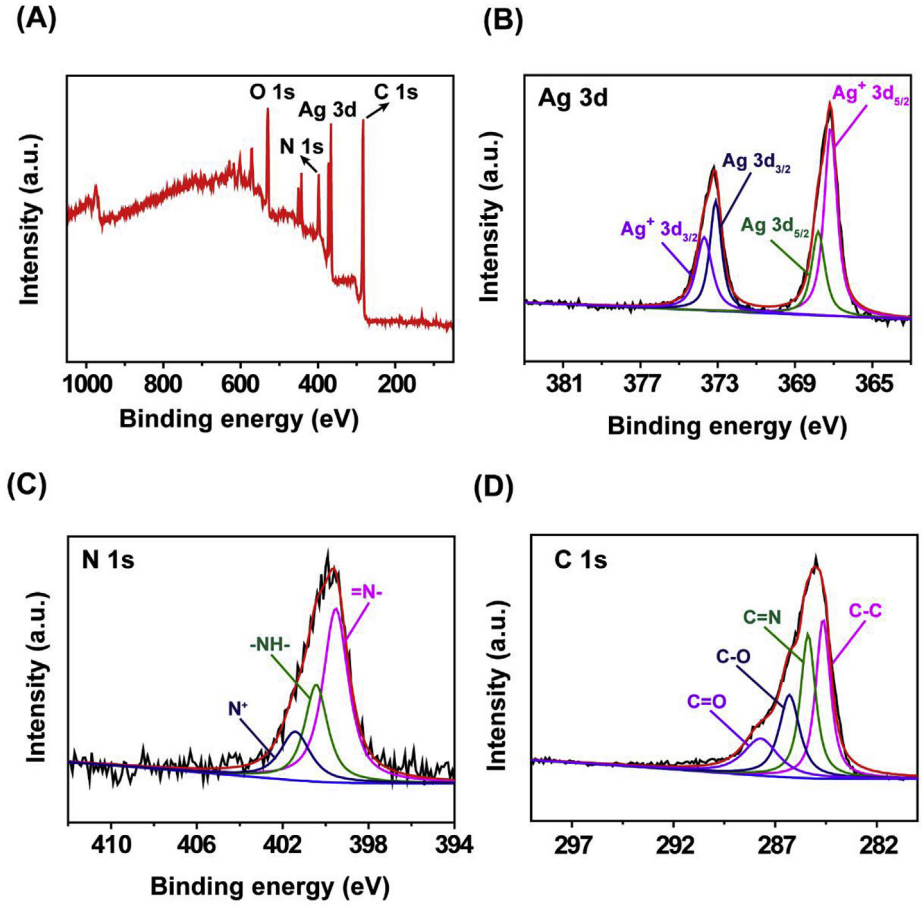

Fig. 2. (A) Full XPS spectra and high resolution XPS spectra of **(B)** Ag 3d, **(C)** N 1s and **(D)** C 1s of ABEI-Ag@PAni-ATMP.

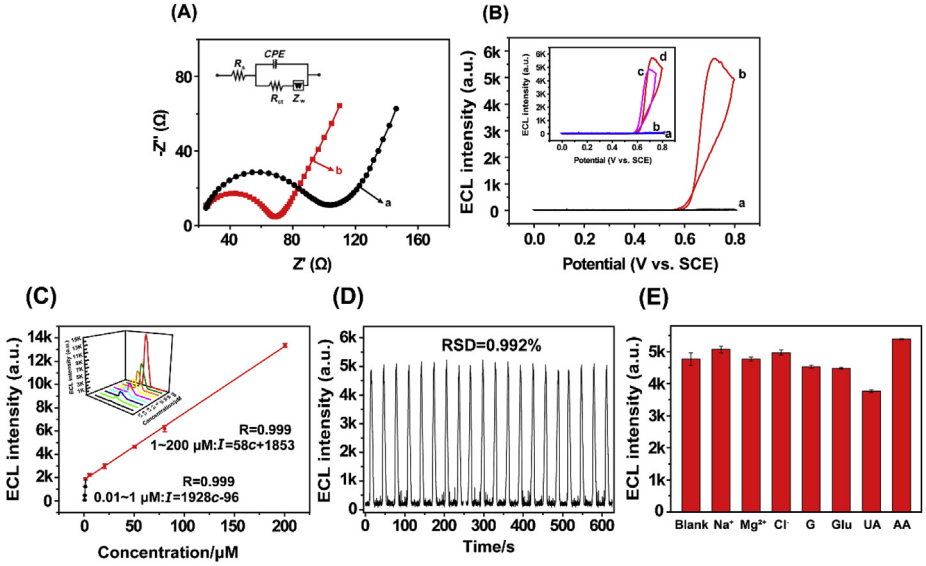

Fig. 3. (A) EIS of (a) Ani-ATMP modified GCE and (b) PAni-ATMP modified GCE in 5 mM $[Fe(CN)_6]^{4-/3-}$ containing 0.1 M KCl solution. **(B)** ECL-potential curve of ABEI-Ag@PAni-ATMP in 0.1 M PBS (pH = 8.0) solution in the (a) absence and (b) presence of 20 μM H_2O_2. Inset: (a) bare GCE, (b) PAni-ATMP, (c) ABEI-Ag and (d) ABEI-Ag@PAni-ATMP in the presence of 20 μM H_2O_2 with a scan rate of 50 mV s^{-1}. **(C)** The calibration plot for xanthine detection in the range of 0.1–200 μM. Inset: ECL response of the ABEI-Ag@PAni-ATMP modified GCE toward different concentrations of xanthine (0.1, 0.3, 0.7, 1, 5, 20, 50, 80, and 200 μM). **(D)** Stability of the ABEI-Ag@PAni-ATMP based ECL biosensor in the presence of 50 μM xanthine. **(E)** Selectivity of the ECL selectivity measured in blank, Na^+, Mg^{2+}, Cl^-, G, Glu, UA, and AA under the same conditions. The concentration of each interfering substances is 50 μM.

regression equation and squared correlation coefficient were I (a.u.) = 58c + 1853 and 0.999, respectively. The detection limit was estimated to be 9.6 nM. A comparison with other xanthine sensors reported in the literature were shown in Table 1. It seems obvious that our proposed ECL biosensor was able to offer a wider linear range with a lower detection limit. As shown in Fig. 3D, by incubating xanthine with 50 μM for continuous scans of 20 cycles, the stability was explored to show a relative standard deviation (RSD) of 0.992% which suggested an excellent stability. These results indicated that our proposed biosensor can be applied to detect xanthine in fish samples. Furthermore, the influence of the presence of various interfering substances such as Na^+, Mg^{2+}, Cl^-, G, Glu, UA, and AA at their physiological normal level response to xanthine (50 μM) was examined. As shown in Fig. 3E, the introduction of Na^+, Mg^{2+}, Cl^-, G and Glu has a negligible effect on the ECL signal. However, the ECL responses of UA and AA were obviously fluctuated due to their combination to a low oxidization

Table 1
Different Methods for Xanthine Detection

Electrode material	Method	Detection range (μM)	Detection limit (nM)	ref
ZnO-NP/CHIT/c-MWCNT/PANI	EC	0.1-100	100	Devi et al. (2012)
XO/layered double hydroxided	EC	1-200	100	Shan et al. (2009b)
AgNPs	EC	2-16	150	Devi et al. (2013)
c-MWCNTs/Fe_3O_4/TCNQ/CHIT/GCE	EC	1.9-230	2.0×10^4	Dalkıran et al. (2017)
PVF + XOD-/Pt	EC	0.43-28.4	520	Wang (2017)
PDDA-CNTs-G	EC	5-50	4.4×10^3	Si et al. (2018)
RB-capped TGA/GNPs	Flu	0.093-8.4	10	Menon and Kumar (2017)
HCPE/XOD	ECL	8-300	3.0×10^3	Lin et al. (2008)
ABEI-Ag@PAni-ATMP	**ECL**	**0.01-200**	**9.6**	**This work**

Table 2
Xanthine Determination Results in fish samples.

Sample number	added (μM)	found (μM)	recovery (%)
1	10	9.86 ± 0.56	98.6
2	20	18.85 ± 1.56	94.3

potential. This indicates that the as-prepared ECL immunosensor has excellent selectivity toward xanthine detection.

In order to check the reproducibility, reuse stability of our proposed xanthine biosensor, the xanthine content in same fish sample was examined with six electrodes and again after storage at 4 °C for one week. The results showed that determinations were almost consistent and RSD for fish sample determination were 4.8% and 5.2%, respectively, showing the good reproducibility and reuse stability of our sensor. Furthermore, the electrode lost only 20% of its initial response after two weeks of storage. Good long-term stability of the XOD modified ABEI-Ag@PAni-ATMP electrode can be attributed to the enzyme immobilization matrix ABEI-Ag@PAni-ATMP conductive polymer hydrogel, which promoted fast electron transfer between electrode and the active site of the XOD.

3.5. Analysis of fish samples

To evaluate the application potential of the proposed biosensor, we used our synthesized biosensor based on ABEI-Ag@PAni-ATMP conductive polymer hydrogel to detect the xanthine released from fish samples. ECL signals of 10 μL fish target solution in 0.1 M PBS, were used to examine the xanthine content under optimized conditions, and the data were shown in Table 2. The percent recovery values range from 94.3% to 98.6%. These results demonstrated that our designed biosensor is feasible in the determination of xanthine content in fish samples.

4. Conclusions

In summary, a novel enhanced solid-state ECL xanthine biosensor was constructed by immobilizing XOD onto ABEI-Ag@PAni-ATMP conductive polymer hydrogel. Benefiting from the excellent conductivity, high surface reaction activity and strong adsorption ability of PAni-ATMP conductive polymer hydrogel, the ABEI-Ag@PAni-ATMP conductive polymer hydrogel showed remarkable ECL performance by using H_2O_2 as co-reactant. In addition, the XOD can be stably immobilized on ABEI-Ag@PAni-ATMP conductive polymer hydrogel which has a unique ability to promote fast electron transfer between electrode and the active site of the XOD. Two linear ranges were obtained in the concentration range of 0.01–1 μM and 1–200 μM with the LOD of 9.6 nM (S/N = 3). In addition, the reliable recovery (94.3%–98.6%) and reasonable RSD (0.56%–1.56%) in the analysis of fish samples. However, its application in clinical testing is still a huge challenge. Meanwhile, the interference from ascorbic acid remained to be resolved. Our proposed xanthine biosensor exhibits a great application potential for the detection of other clinical diagnostic and therapeutic analytes.

Notes

The authors declare no competing financial interest.

Declaration of competing interest

The authors declare that they have no known competing financial interests or personal relationships that could have appeared to influence the work reported in this paper.

CRediT authorship contribution statement

Lian-Hua Xu: Data curation, Investigation, Formal analysis, Methodology, Writing - original draft, Writing - review & editing. **Jun-ji Li:** Data curation, Investigation, Formal analysis, Methodology, Writing - original draft, Writing - review & editing. **Hai-Bo Zeng:** Conceptualization, Formal analysis, Writing - review & editing. **Xue-Ji Zhang:** Conceptualization, Formal analysis, Funding acquisition, Methodology, Project administration, Writing - review & editing. **Serge Cosnier:** Conceptualization, Formal analysis, Writing - review & editing. **Robert S. Marks:** Conceptualization, Formal analysis, Funding acquisition, Methodology, Project administration, Writing - review & editing. **Dan Shan:** Conceptualization, Formal analysis, Funding acquisition, Methodology, Project administration, Writing - review & editing.Acknowledgements

This research was supported by National Natural Science Foundation of China (Grant No.21675086), the Fundamental Research Funds for the Central Universities (No.30918012202), “Overseas Academic Partnership Program” of Nanjing University of Technology, and a project founded by the priority academic program development of Jiangsu Higher Education Institutions (PAPD). The authors wish also to acknowledge the support from the Sino-French international research network “New nanostructured materials and biomaterials for renewable electrical energy sources” for providing facilities.

Conflict of interest

The authors declare that they have no known competing financial interests or personal relationships that could have appeared to influence the work reported in this paper.

Appendix A. Supplementary data

Supplementary data to this article can be found online at https://doi.org/10.1016/j.bios.2019.111601.

References

Abu-Rabeah, K., Polyak, B., Ionescu, R.E., Cosnier, S., Marks, R.S., 2005. Biomacromolecules 6, 3313–3318.

Burge, S., Parkinson, G.N., Hazel, P., Todd, A.K., Neidle, S., 2006. Nucleic Acids Res. 34, 5402–5415.
Cai, W.R., Zhang, G.Y., Lu, K.K., Zeng, H.B., Cosnier, S., Zhang, X.J., Shan, D., 2017. ACS Appl. Mater. Interfaces 9, 20904–20912.
Choi, J., Jang, S.K., Kim, F.S., 2018. Phys. Status Solidi A 215, 1701019.
Dalkıran, B., Erden, P.E., Kılıç, E., 2017. Talanta 167, 286–295.
Devi, R., Batra, B., Lata, S., Yadav, S., Pundir, C.S., 2013. Process Biochem. 48, 242–249.
Devi, R., Yadav, S., Pundir, C.S., 2012. Analyst 137, 754–759.
He, Y., Liu, D., He, X., Cui, H., 2011. Chem. Commun. 47, 10692–10694.
Hoffmann, T., Friedel, P., Harnisch, C., Häußler, L., Pospiech, D., 2012. J. Anal. Appl. Pyrolysis 96, 43–53.
Huang, S., He, Q., Xu, S., Wang, L., 2015. Anal. Chem. 87, 5451–5456.
Jiang, P., Li, S.Y., Xie, S.S., Gao, Y., Song, L., 2004. Chem. Eur J. 10, 4817–4821.
Jiang, X., Wang, H., Wang, H., Yuan, R., Chai, Y., 2016. Anal. Chem. 88, 9243–9250.
Jiang, X., Wang, H., Yuan, R., Chai, Y., 2018. Anal. Chem. 90, 8462–8469.
Juskowiak, B., 2006. Anal. Chim. Acta 568, 171–180.
Kalimuthu, P., Leimkuhler, S., Bernhardt, P.V., 2012. Anal. Chem. 84, 10359–10365.
Li, G., Yu, X., Liu, D., Liu, X., Li, F., Cui, H., 2015. Anal. Chem. 87, 10976–10981.
Li, S.K., Liu, Z.T., Li, J.Y., Chen, A.Y., Chai, Y.Q., Yuan, R., Zhuo, Y., 2018. ACS Appl. Mater. Interfaces 10, 14483–14490.
Lin, Z., Sun, J., Chen, J., Guo, L., Chen, Y., Chen, G., 2008. Anal. Chem. 80, 2826–2831.
Liu, Z.T., Li, S.K., Wei, R.T., Chen, A.Y., Chai, Y.Q., Yuan, R., Zhuo, Y., 2018. Sens. Actuators, B 274, 110–115.
Menon, S., Kumar, K.G., 2017. LWT - Food Sci. Technol. (Lebensmittel-Wissenschaft -Technol.) 86, 8–13.
Naqash, W., Majid, K., 2017. J. Mater. Sci. Mater. Electron. 28, 14217–14225.
Niu, Y., 2006. Polym. Compos. 27, 627–632.
Shan, D., Wang, Y., Xue, H., Cosnier, S., 2009a. Sens. Actuators, B 136, 510–515.
Shan, D., Wang, Y., Zhu, M., Xue, H., Cosnier, S., Wang, C., 2009b. Biosens. Bioelectron. 24, 1171–1176.
Si, Y., Park, J.W., Jung, S., Hwang, G.S., Goh, E., Lee, H.J., 2018. Biosens. Bioelectron. 121, 265–271.
Stulz, E., Clever, G., Shionoya, M., Mao, C., 2011. Chem. Soc. Rev. 40, 5633–5635.
Wang, H.S., 2017. Coord. Chem. Rev. 349, 139–155.
Wang, S., Zhao, Y., Wang, M., Li, H., Saqib, M., Ge, C., Zhang, X., Jin, Y., 2019. Anal. Chem. 91, 3048–3054.
Wang, X.X., Wu, Q., Shan, Z., Huang, Q.M., 2011. Biosens. Bioelectron. 26, 3614–3619.
Wang, Z., Ma, B., Shen, C., Lai, O.M., Tan, C.P., Cheong, L.Z., 2019. Food Anal. Methods 12, 1715–1724.
Wang, Z., Yan, Z., Sun, N., Liu, Y., 2015. Biosens. Bioelectron. 68, 771–776.
Wu, G., Li, L., Li, J.H., Xu, B.Q., 2006. J. Power Sources 155, 118–127.
Xue, G., Yu, W., Yutong, L., Qiang, Z., Xiuying, L., Yiwei, T., Jianrong, L., 2019. Anal. Methods 11, 1021–1026.
Yang, H.Y., Wang, H.J., Xiong, C.Y., Chai, Y.Q., Yuan, R., 2017. ACS Appl. Mater. Interfaces 9, 36239–36246.
Zhuang, R.F., Liu, X.L., Dai, A.B., 1985. J. Inorg. Chem. 1, 52–60.